DØ Note 6387-CONF

Constraints on the $J^P = 2^+$ hypothesis for the 125 GeV boson in $W/Z + b\bar{b}$ final states at the D0 Experiment

The DØ Collaboration
URL http://www-d0.fnal.gov
(Dated: September 13, 2013)

We present a study of the spin J and parity P of a resonance X with a mass of 125 GeV produced in association with a W or Z boson in final states with two b-quarks with the D0 experiment at the Fermilab Tevatron collider. We compare the standard model Higgs boson hypothesis, $J^P = 0^+$, with an alternative hypothesis, $J^P = 2^+$ in $\ell\nu b\bar{b}$, $\ell\ell b\bar{b}$, and $\nu\nu b\bar{b}$ final states that are sensitive to WX and ZX production with $X \to b\bar{b}$. We use a likelihood ratio to compute the level of preference in the data for the $J^P = 2^+$ case relative to the standard model. We reject the hypothesis of $J^P = 2^+$ with graviton-like couplings at the 99.9% C.L., or 3.1 s.d., assuming a signal production cross section equal to the best-fit value as measured in our data for the standard model Higgs boson search. Assuming a signal production cross section times branching ratio equal to the standard model rate, the expected exclusion sensitivity is 3.1 s.d. We also consider that our data excess could be due to an admixture of a SM Higgs and a $J^P = 2^+$ signal and exclude $J^P = 2^+$ fractions above 0.57 at the 95% C.L.

Preliminary Results for the 2013 Summer Conferences
Updated for Fall 2013 - see errata

Errata

We found a software bug in the code used in the previous note for the statistical analysis when contributions from both $J^P = 0^+$ and $J^P = 2^+$ are present. We have recalculated the LLR and CL_s as a function of the 2^+ fraction, f_{2^+}, as shown in the revised Fig. 10. The observed lower limits on f_{2^+} changed from 0.42 to 0.57 for the case $\mu = 1.23$ and from 0.56 to 0.71 for the case $\mu = 1.0$. Figures 8 and 9 have been updated using larger numbers of pseudoexperiments.

I. INTRODUCTION

After the discovery of a new boson in searches for the Higgs boson, H, at the CERN Large Hadron Collider (LHC) [1, 2] in bosonic decay modes, and the evidence for the decay to a pair of b-quarks at the Tevatron experiments [3], it is crucial to determine the new particle's properties using all available final states. The standard model (SM) predicts that the Higgs boson is a CP-even spin-0 particle ($J^P = 0^+$). The observation of a two-photon decay $H \to \gamma\gamma$ at the LHC precludes spin 1 according to the Landau-Yang Theorem [4, 5]. Results from the ATLAS and CMS experiments have constrained $J^P = 0^-$ and $J^P = 2^+$ in the $H \to \gamma\gamma$, $H \to WW \to \ell\nu\ell\nu$ and $H \to ZZ \to 4\ell$ final states [6, 7, 8] but have not yet tested the J^P of the new particle in the $b\bar{b}$ final state. The $J^P = 2^+$ hypothesis is excluded at the 3.7 (2.8) sigma level by ATLAS (CMS) when combining all bosonic decay modes, while their expected exclusion sensitivity is 3.0 (3.1) s.d. In this Note we present a study of the particle decaying in a fermionic decay mode $H \to b\bar{b}$ under the hypothesis that the new boson is a $J^P = 2^+$ particle with graviton-like couplings, and we compare it to the SM assignment of $J^P = 0^+$. This is the first time that a study of the J^P of the new boson in fermionic decay mode is presented. We also examine the maximum fraction of our signal that can be ascribed to a $J^P = 2^+$ signal. Work continues to test the $J^P = 0^-$ hypothesis.

Searches for associated production of a Higgs and vector boson $V (V = W, Z)$ are sensitive to the different kinematics of the various J^P combinations in several observables, particularly in the invariant mass of the $Vb\bar{b}$ system [9]. The $VH \to Vb\bar{b}$ searches are well-suited to discriminate between the $J^P = 0^+$ of the SM Higgs and the non-SM scenarios. We use the most recent $WH \to \ell\nu b\bar{b}$ ($\ell = e, \mu$) [10], $ZH \to \ell\ell b\bar{b}$ [11], and $ZH \to \nu\bar{\nu}b\bar{b}$ [12] searches using the D0 detector with no modifications to the event selections or kinematic cuts.

II. THE D0 DETECTOR

The D0 detector is described in detail elsewhere [13, 14, 15], and here we present a brief overview. The innermost system is the central tracking system, consisting of a silicon microstrip tracker (SMT) and a central fiber tracker (CFT). They are located within a 2 T superconducting solenoidal magnet, and their designs are optimized for tracking and vertexing at pseudorapidities $|\eta| < 3$ for the SMT and $|\eta| < 2.5$ for the CFT. A liquid-argon and uranium calorimeter has a central section (CC) covering pseudorapidities up to ≈ 1.1, and two end calorimeters (EC) that extend coverage to $|\eta| \approx 4.2$, with all three housed in separate cryostats. An outer muon system, covering $|\eta| < 2$, consists of a layer of tracking detectors and scintillation trigger counters in front of 1.8 T solid iron toroids, followed by two similar layers after the toroids. Luminosity is measured using plastic scintillator arrays placed in front of the EC cryostats. The trigger and data acquisition systems are designed to accommodate the luminosities of the Tevatron.

III. DATA AND SIMULATED SAMPLES

We use 9.5–9.7 fb^{-1} of integrated luminosity collected with the D0 experiment satisfying relevant data-quality requirements in each of the three channels [10, 11, 12]. The SM background processes are either estimated from dedicated data samples (multijet backgrounds), or from Monte Carlo (MC) simulation. The V+jets and $t\bar{t}$ processes are generated using ALPGEN [16], single top processes are generated using SINGLETOP [17], and diboson (VV) processes are generated using PYTHIA [18]. The SM Higgs boson processes are also produced using PYTHIA. The signal samples for the $J^P = 2^+$ hypothesis for this analysis are generated using MADGRAPH 5 version 1.4.8.4 [19]. We have verified that $J^P = 0^+$ samples produced with MADGRAPH agree well with our existing SM PYTHIA simulations. Within MADGRAPH there are several non-SM models available, as well as the ability to implement user-defined models. For this analysis, we follow the prescription described in Ref. [9]. The $J^P = 2^+$ signal samples were created using the Randall-Sundrum (RS) model, an extra-dimension model with a massive $J^P = 2^+$ particle that has graviton-like couplings. These new states are introduced via new dimension-five operators [20, 21]:

$$\mathcal{L}_{2^+} = \frac{c_V^G}{\Lambda} G^{\mu\nu} T^V_{\mu\nu}, \tag{1}$$

where $G^{\mu\nu}$ represents the $J^P = 2^+$ particle, $T^V_{\mu\nu}$ the stress-energy tensor of the vector boson, Λ the effective Planck mass, and the c_V^G terms are functions of the overlap of the graviton resonance with the vector boson SM fields in the bulk of the extra dimension. The mass of the non-SM Higgs-like particle X was set to 125 GeV, a value close to the mass measured by the LHC experiments [1, 2] . We simulate X decays to a pair of b-quarks only, and for our initial sample normalization we assume that the cross section of the VX production times the branching ratio,

$\sigma(VX) \times \mathcal{B}(X \to b\bar{b})$, is equal to the SM Higgs boson value of 0.12 pb. The PDF set used was CTEQ6L1. We do not apply additional kinematic cuts to the final-state particles during sample generation. These samples are then subjected to parton showering with PYTHIA and processed through the standard D0 full detector simulation and reconstruction programs.

IV. SUMMARY OF CONTRIBUTING ANALYSES

We begin with the three published $H \to b\bar{b}$ search analyses, the $WH \to \ell\nu b\bar{b}$ search analysis [10], the $ZH \to \ell\ell b\bar{b}$ search analysis [11], and the $ZH \to \nu\bar{\nu}b\bar{b}$ search analysis [12]. All analyses employ a b-tagging algorithm to identify jets that are consistent with the b-quark lifetime and fragmentation. This algorithm provides improved performance over an earlier neural network algorithm [22].

The $WH \to \ell\nu b\bar{b}$ analysis selects events with a charged lepton (electron or muon), significant imbalance in the transverse energy ($\not\!\!E_T$), and two or three jets (j). Using the average of the two highest outputs from the b-tagging algorithm for all selected jets, events are divided into four orthogonal b-tagging categories, "one-tight-tag" (1TT), "two-loose-tag" (2LT), "two-medium-tag" (2MT), and "two-tight-tag" (2TT). A boosted decision tree (BDT), trained separately for each jet multiplicity and b-tag category, serves as the final discriminant in the SM Higgs boson search. In the J^P analysis the 3-jet channels bring negligible additional sensitivity and we do not consider them further.

The $ZH \to \ell\ell b\bar{b}$ analysis selects events with two isolated charged leptons and at least two jets. A kinematic fit corrects the measured jet energies to their best fit values according to the constraints that the dilepton invariant mass should be consistent with the Z boson mass M_Z [23] and the total transverse momentum of the leptons and jets is consistent with zero. The events are further divided into orthogonal "single-tag" (ST) and "double-tag" (DT) subchannels according to the number of b-tagged jets. The analysis uses random forest (RF) [24] discriminants to provide distributions for the final statistical analysis in the SM Higgs boson search. The first RF discriminant is designed to discriminate against $t\bar{t}$ events, and divides events into $t\bar{t}$-enriched and $t\bar{t}$-depleted regions, while the second provides the final variable. In this study we consider only events in the $t\bar{t}$-depleted ST and DT regions.

The $ZH \to \nu\bar{\nu}b\bar{b}$ analysis selects events with large $\not\!\!E_T$ and exactly two jets. This search is also sensitive to the WH process when the charged lepton from $W \to \ell\nu$ decay is not identified. A dedicated decision tree designed to reject background events from multijet production is employed to provide additional rejection of the otherwise large multijet background. Two orthogonal b-tagging subchannels, medium (MT), and tight (TT), are defined using the sum of the b-tagging discriminant outputs from the two jets. BDT classifiers, trained separately for the different b-tagging categories, are the final discriminants in the SM Higgs boson search.

The three analyses have been combined and included as inputs to the D0 SM Higgs boson search [25], and exhibit an excess over the SM background expectation that is consistent with a Higgs boson signal. The best fit to data for the signal cross section for the three $b\bar{b}$ analyses is $1.23^{+1.24}_{-1.17}$ times the SM prediction.

V. SIGNAL OPTIMIZATION

We use the invariant (transverse) mass distribution to discriminate between different J^P signal hypotheses in the final statistical analysis. For the $\ell\ell b\bar{b}$ final state we use the invariant mass of the two leptons and two jets with the highest b-tag output (DT), or the b-tagged jet and the leading p_T non-tagged jet (ST), $M_{\ell\ell jj}$. For the $\ell\nu b\bar{b}$ final state we use the transverse mass of the ℓ, $\not\!\!E_T$, and two jets, and for the $\nu\bar{\nu}b\bar{b}$ final state we use the transverse mass of the $\not\!\!E_T$ and two jets. The transverse mass is defined as:

$$M_T = \sqrt{E_T^2 - \overrightarrow{p_T}^2}, \tag{2}$$

where E_T and $\overrightarrow{p_T}$ are the total transverse energy and transverse momentum of the system, respectively. Figure 1 shows the separation between SM Higgs boson signal ($J^P = 0^+$) from models with $J^P = 0^-$ and $J^P = 2^+$ for the $WH \to \ell\nu b\bar{b}$, $ZH \to \ell\ell b\bar{b}$, and $ZH \to \nu\bar{\nu}b\bar{b}$ processes.

While these variables discriminate between spin and parity assignments very well for the signals, they do not separate SM signal well from backgrounds due to other SM processes, as can be seen in Figure 2 for the $\ell\nu b\bar{b}$, $\ell\ell b\bar{b}$, and $\nu\bar{\nu}b\bar{b}$ final states. To discriminate against SM backgrounds we use the invariant mass, M_{jj}, of the two leading b-tagged jets (or b-tagged jet and leading non-tagged jet if only one jet is tagged) for the $\ell\ell b\bar{b}$ and $\nu\bar{\nu}b\bar{b}$ final states, or final multivariate discriminant output (MVA) used in the SM Higgs boson search for $\ell\nu b\bar{b}$ final state [10], as shown in Figure 3, to provide discrimination against SM backgrounds.

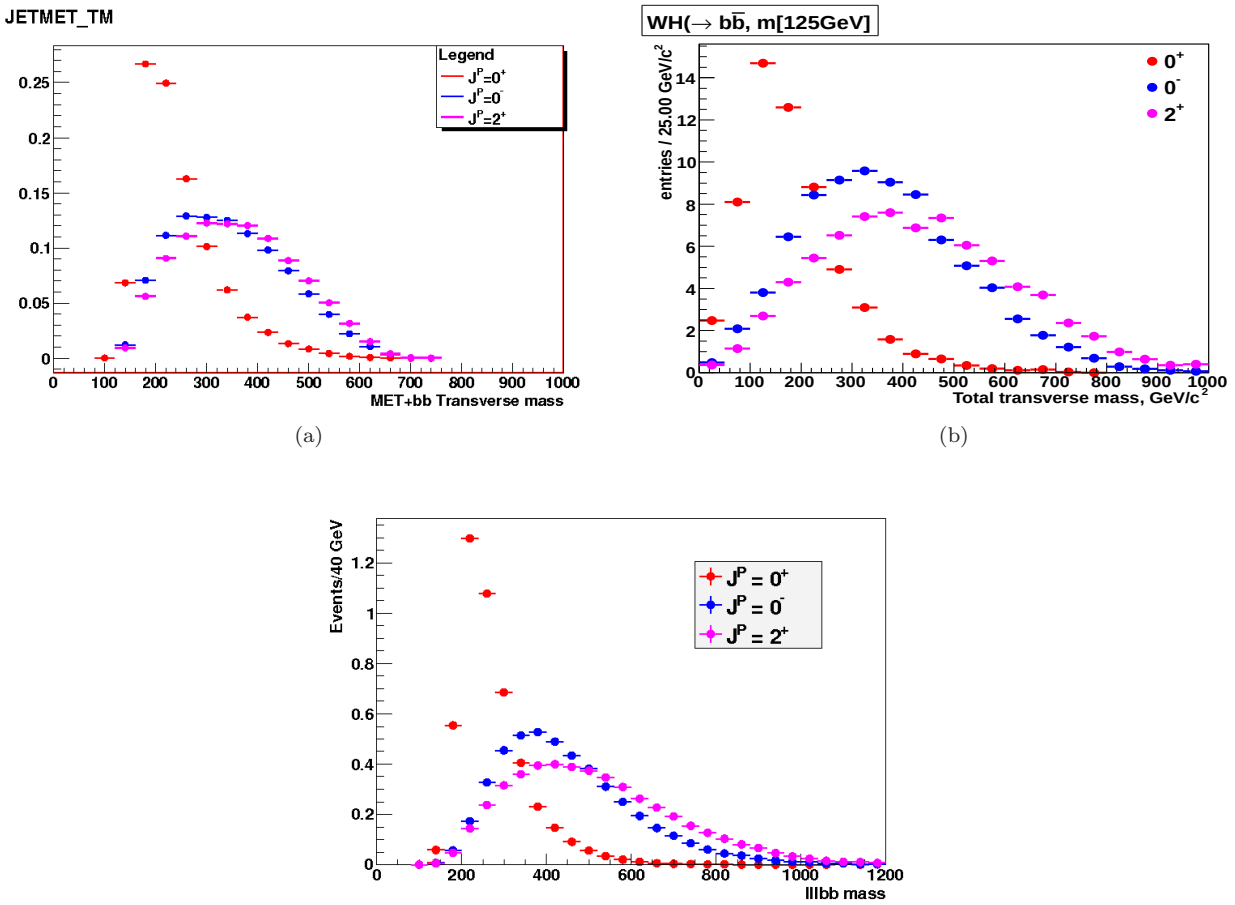

FIG. 1: Transverse mass of the: (a) $\nu\nu b\bar{b}$ system for the three spin states, (b) $\ell\nu b\bar{b}$ system, and (c) invariant mass of the $\ell\ell b\bar{b}$ system for simulated events after all selection cuts. All histograms are normalized to have unit area. All signals assume $M_H = 125$ GeV.

In the case of the $\ell\ell b\bar{b}$ and $\nu\bar{\nu}b\bar{b}$ analyses we select two regions with different signal purity. Events with $100 \leq M_{jj} \leq 160$ ($70 \leq M_{jj} \leq 150$) for the $\ell\ell b\bar{b}$ ($\nu\bar{\nu}b\bar{b}$) analysis comprise the "high-purity" or HP region, while the rest of the events are part of the "low-purity" or LP region.

In the $\ell\nu b\bar{b}$ analysis events with MVA ≤ 0 provide negligible sensitivity to the analysis and are not considered further. We split the remaining events into LP and HP regions, with $0 <$ MVA ≤ 0.5 defining the LP region and MVA > 0.5 defining the HP region. Figure 4 shows the $M_{\ell\ell jj}$ distribution for ST and DT events in the $\ell\ell b\bar{b}$ analysis. Figure 5 shows the M_T distribution for MT and TT events in the $\nu\bar{\nu}b\bar{b}$ analysis. Figures 6 and 7 show the M_T distribution for 1TT, 2LT, 2MT, and 2TT events in the $\ell\nu b\bar{b}$ analysis for the LP and HP regions, respectively. Each region is a separate input channel in the final statistical analysis.

VI. STATISTICAL ANALYSIS

We combine results using the CL_s method with a negative log-likelihood ratio (LLR) test statistic for the two hypotheses, the test hypothesis, H_1, and the null hypothesis, H_0 [25, 26, 27, 28]. The LLR is given by:

$$\text{LLR} = -2\ln(L_{H_1}/L_{H_0}), \tag{3}$$

where L_x is the likelihood function for the hypothesis x. We define CL_s as:

$$CL_s = CL_{H_1}/CL_{H_0} \tag{4}$$

where CL_x for a given hypothesis x is defined using the conditional probability:

$$CL_x = P(\mathrm{LLR} \geq \mathrm{LLR}^{obs}|x) \tag{5}$$

These confidence levels are evaluated by integrating the corresponding LLR distributions of simulated experiment outcomes drawn from Poisson distributions of the relevant signal and background parameters. Separate channels and bins are combined by summing LLR values over all bins and channels. This method provides a robust means of combining channels while maintaining each individual channel's sensitivity and different systematic uncertainties. Systematic uncertainties are treated as nuisance parameters with Gaussian probability distributions constrained by their priors. This approach ensures that the uncertainties and their correlations are propagated to the outcome with their appropriate weights.

To minimize the degrading effects of systematic uncertainties on the search sensitivity, we fit the individual background contributions to the observed data by maximizing a likelihood function [28]. The likelihood is a joint Poisson probability over the number of bins in the calculation and is a function of the nuisance parameters and their uncertainties. The maximization of the likelihood function is performed over the nuisance parameters, with separate fits performed to both the H_0 and H_1 hypotheses for each Poisson MC trial. We have verified that all fit parameters and pulls on the systematic uncertainties are well-behaved.

VII. SYSTEMATIC UNCERTAINTIES

Systematic uncertainties on signal and backgrounds vary among the analyses and are described in detail in Refs. [10, 11, 12]. We summarize only the major components below. The $\ell\nu b\bar{b}$ and $\nu\bar{\nu}b\bar{b}$ analyses, along with the signals in the $ZH \to \ell\ell b\bar{b}$ analysis, have an uncertainty of 6.1% from the integrated luminosity [29], while the overall normalization in the $ZH \to \ell\ell b\bar{b}$ analysis is determined from the $Z \to \ell\ell$ mass peak in data assuming the NNLO Z/γ^* cross section, reducing the uncertainty to about 1%. An uncertainty of 1–10% due to the uncertainty on the b-tagging rate, depending on the number and quality of tagged jets is taken into account. All analyses take into account uncertainties on jet-energy scale, resolution, and jet identification efficiency, for a combined uncertainty of $\approx 7\%$. They also account for uncertainties associated with measurement and acceptances for leptons, which range from 1% to 9% depending on the final state. The largest contribution to all analyses is from the uncertainties on the cross sections of the simulated $W/Z+$ heavy flavor backgrounds which are 20–30%. All other cross section uncertainties of simulated backgrounds are below 10%. These values include both the uncertainty on the theoretical cross section calculations and the uncertainties on the higher-order correction factors. The uncertainty on the expected multijet background in each channel is dominated by the statistics of the data sample from which it is estimated. It is considered separately from the uncertainties on the cross sections of the simulated backgrounds, and ranges from 10% to 30%. However, this does not have a large impact on the sensitivity of this analysis since the multijet background is small in the high-purity regions. All analyses take into account the uncertainties on the differential cross sections arising from the choice of PDF set and QCD scale. In addition, we incorporate uncertainties that alter differential distributions and kinematics of the dominant backgrounds in the analyses. These uncertainties are estimated from the variation of the final discriminant distribution due to generator and background modeling uncertainties. Correlations between systematic sources are also carried through in the calculations. For example, the uncertainty on the integrated luminosity is taken to be fully correlated between all signals and backgrounds obtained from simulation. Hence any fluctuation in luminosity is common to all channels for a single pseudoexperiment. All systematic uncertainties originating from a common source are assumed to be fully correlated.

VIII. RESULTS

In the first part of our statistical analysis we define the null hypothesis H_0 as the sum of SM background processes and the SM Higgs boson. The corresponding test hypothesis H_1 assumes the presence of a boson with $J^P = 2^+$ plus the SM backgrounds, with no contribution from the SM Higgs boson. We can then define the quantities CL_{0^+} and CL_{2^+} according to Eq. 5. Figure 8 shows the LLR distributions for the three analyses and the combination when comparing the $J^P = 2^+$ and $J^P = 0^+$ hypotheses. Table I shows the 95% C.L. limits on $J^P = 2^+$ production in the individual analyses and combination in units of SM cross section, σ_{SM}, under these assumptions. When calculating the limits, we hold the $J^P = 0^+$ cross section fixed at the SM value. The 95% C.L. limits represent the value of μ, the Higgs boson signal strength [25], at which the given channels reach a $1 - CL_s$ value of 0.95, i.e., exclude the non-SM hypothesis in favor of the SM hypothesis at 95% C.L. The sensitivity obtained for the $J^P = 2^+$ hypothesis is significantly higher than the sensitivity obtained for the SM hypothesis.

Table II lists the CL_{2^+}, CL_{0^+}, and $1-CL_s$ results, where we calculate the CL_s values using two different signal cross sections expressed as $\mu \times \sigma_{SM}$. We consider $\mu = 1.23$, corresponding to the best fit value $VH \to Vb\bar{b}$ rate in our data [25], and $\mu = 1.0$, corresponding to the SM cross section. Figure 9 shows the LLR distributions for the three analyses and the combination when comparing the $J^P = 2^+$ and $J^P = 0^+$ hypotheses for $\mu = 1.23$. We can also calculate expected values for each of these quantities by replacing $\mathrm{LLR}^{\mathrm{obs}}$ with $\mathrm{LLR}^{\mathrm{exp}}_{0^+}$, the median expectation for the $J^P = 0^+$ hypothesis. We interpret the $1-CL_s$ values as the confidence level at which we exclude the $J^P = 2^+$ hypothesis in favor of the SM prediction of $J^P = 0^+$ for the given value of μ. For the $\mu = 1.23$ case we exclude the $J^P = 2^+$ hypothesis at the 99.9% C.L. i.e., at the 3.1 s.d. level. For the $\mu = 1.0$ case we exclude the $J^P = 2^+$ hypothesis at the 99.2% C.L. The expected exclusion, obtained when assuming $\mu = 1.0$ for both the $J^P = 2^+$ and $J^P = 0^+$ signals is at the 99.9% C.L. i.e. at the 3.1 s.d. level.

Channel	$WH \to \ell\nu bb$	$ZH \to \ell\ell bb$	$ZH \to \nu\nu bb$	Combined
	$J^P = 2^+$ vs. $J^P = 0^+$			
Exp. Lim. σ^{2^+}/σ_{SM}	1.01	1.59	1.15	0.49
Obs. Lim. σ^{2^+}/σ_{SM}	1.56	1.76	1.02	0.73

TABLE I: 95% C.L. upper limits on $J^P = 2^+$ associated production as a ratio to the SM Higgs associated production cross section times $H \to b\bar{b}$ branching fraction, taking the null hypothesis H_0 to be SM Higgs boson signal plus background, and test hypothesis H_1 to be $J^P = 2^+$ signal plus background.

Channel	$WH \to \ell\nu b\bar{b}$	$ZH \to \ell\ell b\bar{b}$	$ZH \to \nu\nu b\bar{b}$	Combined
	$J^P = 2^+$ vs. $J^P = 0^+$			
CL_{2^+} Exp. ($\mu = 1.00$)	0.015	0.080	0.035	0.0004
CL_{0^+} Exp. ($\mu = 1.00$)	0.5	0.5	0.5	0.5
CL_{2^+} Obs. ($\mu = 1.00$)	0.153	0.154	0.017	0.0066
CL_{0^+} Obs. ($\mu = 1.00$)	0.847	0.693	0.359	0.8487
1-CL_s Exp. ($\mu = 1.00$)	0.946	0.840	0.926	0.9992
1-CL_s Obs. ($\mu = 1.00$)	0.831	0.778	0.948	0.9922
CL_{2^+} Exp. ($\mu = 1.23$)	0.005	0.052	0.021	0.0001
CL_{0^+} Exp. ($\mu = 1.23$)	0.5	0.5	0.5	0.5
CL_{2^+} Obs. ($\mu = 1.23$)	0.013	0.097	0.008	0.0010
CL_{0^+} Obs. ($\mu = 1.23$)	0.903	0.675	0.346	0.8526
1-CL_s Exp.($\mu = 1.23$)	0.975	0.897	0.958	0.9999
1-CL_s Obs.($\mu = 1.23$)	0.893	0.857	0.976	0.9988

TABLE II: Expected and observed CL_s values (assuming signal cross sections equal to the 125 GeV SM Higgs production cross section times μ), taking the null hypothesis H_0 to be SM Higgs boson signal plus background, and test hypothesis H_1 to be $J^P = 2^+$ signal plus background.

We also consider the possibility of multiple signals in the final state, i.e. an admixture of $J^P = 0^+$ and $J^P = 2^+$. For this study we fix the sum of the two cross sections to a specific value of $\mu \times \sigma_{SM}$, and vary the fraction f_{2^+} of non-SM signal and calculate the same values as above as a function of the fraction. We take H_1 to be the sum of the background, the $J^P = 2^+$ signal normalized to $\mu \times \sigma_{SM} \times f_{2^+}$, and the $J^P = 0^+$ signal normalized to $\mu \times \sigma_{SM} \times (1 - f_{2^+})$; accordingly H_0 is then the sum of background and the $J^P = 0^+$ signal normalized to $\mu \times \sigma_{SM}$. Figure 10 shows the LLR, and $1-CL_s$ values as a function of the $J^P = 2^+$ fraction for μ values of 1.0 and 1.23. For $\mu = 1.23$ we exclude fractions $f_{2^+} > 0.57$ at the 95% C.L. In the case of $\mu = 1.0$ we exclude a $J^P = 2^+$ signal fraction above $f_{2^+} > 0.71$.

IX. SUMMARY

We have performed a study of the $J^P = 2^+$ and $J^P = 0^+$ spin and parity assignments of a Higgs-like boson with a mass of 125 GeV produced in association with a W or Z boson in the D0 data. We use the published $WH \to \ell\nu b\bar{b}$, $ZH \to \ell\ell b\bar{b}$, and $ZH \to \nu\bar{\nu}b\bar{b}$ analyses with no modifications to the basic event selection or kinematic cuts. We split the samples into high- and low-purity regions based on dijet mass or MVA output windows. Using the total mass or total transverse mass of the $Vb\bar{b}$ system, we place limits on the cross section times $b\bar{b}$ branching fraction of a $J^P = 2^+$ particle and we quantify the level of preference in data for the $J^P = 0^+$ prediction of the SM. We reject the $J^P = 2^+$ hypothesis where the resonance has graviton-like couplings and cross section times branching ratio to

b-quarks equal to the best-fit value as measured in our data at the 99.9% C.L, or 3.1 standard deviations, in favor of the $J^P = 0^+$ hypothesis. The expected exclusion sensitivity for $J^P = 2^+$ assuming the SM cross section, is 3.1 s.d. When considering a mixing between $J^P = 2^+$ and $J^P = 0^+$ states, we exclude $J^P = 2^+$ fractions above 0.57 at the 95% C.L.

X. ACKNOWLEDGMENTS

We thank the staffs at Fermilab and collaborating institutions, and acknowledge support from the DOE and NSF (USA); CEA and CNRS/IN2P3 (France); MON, NRC KI and RFBR (Russia); CNPq, FAPERJ, FAPESP and FUNDUNESP (Brazil); DAE and DST (India); Colciencias (Colombia); CONACyT (Mexico); NRF (Korea); FOM (The Netherlands); STFC and the Royal Society (United Kingdom); MSMT and GACR (Czech Republic); BMBF and DFG (Germany); SFI (Ireland); The Swedish Research Council (Sweden); and CAS and CNSF (China).

[1] G. Aad *et al.*, [ATLAS Collaboration], Phys. Lett. B **716**, 1 (2012).
[2] S. Chatrchyan *et al.*, [CMS Collaboration], Phys. Lett. B **716**, 30 (2012).
[3] T. Aaltonen *et al.*, [CDF Collaboration and D0 Collaboration], Phys. Rev. Lett. **109**, 071804 (2012).
[4] L. Landau, Dokl.Akad.Nauk Ser.Fiz. **60**, 207 (1948).
[5] C. N. Yang, Phys. Rev. **77**, 242 (1950).
[6] G. Aad *et al.*, [ATLAS Collaboration], arXiv:1307.1432, (2013).
[7] S. Chatrchyan *et al.*, [CMS Collaboration], Phys. Rev. Lett. **110**, 081803 (2013).
[8] S. Chatrchyan *et al.*, [CMS Collaboration], CMS-PAS-HIG-13-005, (2013).
[9] J. Ellis, D. S. Hwang, V. Sanz, and T. You, arXiv:1208.6002, (2012).
[10] V. M. Abazov *et al.*, [D0 Collaboration], arXiv:1301.6122, (2013), accepted by PRD.
[11] V. M. Abazov *et al.*, [D0 Collaboration], arXiv:1303.3276, (2013), accepted by PRD.
[12] V. M. Abazov *et al.*, [D0 Collaboration], Phys. Lett. B **716**, 285 (2012).
[13] V. M. Abazov *et al.*, [D0 Collaboration], Nucl. Instrum. Methods Phys. Res. A **565**, 463 (2006).
[14] M. Abolins *et al.*, Nucl. Instrum. Methods Phys. Res. A **584**, 75 (2008).
[15] R. Angstadt *et al.*, Nucl. Instrum. Methods Phys. Res. A **622**, 298 (2010).
[16] M. L. Mangano, M. Moretti, F. Piccinini, R. Pittau, and A. D. Polosa, J. High Energy Phys. **07**, 001 (2003).
[17] E. E. Boos, V. E. Bunichev, L. V. Dudko, V. I. Savrin, and V. V. Sherstnev, Phys. Atom. Nucl. **69**, 1317 (2006).
[18] T. Sjöstrand, S. Mrenna, and P. Z. Skands, J. High Energy Phys. **05**, 026 (2006).
[19] J. Alwall, M. Herquet, F. Maltoni, O. Mattelaer, and T. Stelzer, J. High Energy Phys. **1106**, 128 (2011).
[20] R. Fok, C. Guimaraes, R. Lewis, and V. Sanz, J. High Energy Phys. **1212**, 062 (2012).
[21] J. Ellis, V. Sanz, and T. You, arXiv:1303.0208, (2013).
[22] V. M. Abazov *et al.*, [D0 Collaboration], Nucl. Instrum. Methods Phys. Res. A **620**, 490 (2010).
[23] J. Beringer *et al.*, Particle Data Group, Phys. Rev. D **86**, 010001 (2012), and 2013 partial update for the 2014 edition.
[24] A. Hoecker *et al.*, PoS **ACAT**, 040 (2007), we use version 4.1.0.
[25] V. M. Abazov *et al.*, [D0 Collaboration], arXiv:1303.0823, (2013), accepted by PRD.
[26] T. Junk, Nucl. Instrum. Methods Phys. Res. A **434**, 435 (1999).
[27] A. L. Read, J. Phys. G **28**, 2693 (2002).
[28] W. Fisher, FERMILAB-TM-2386-E (2007).
[29] T. Andeen *et al.*, FERMILAB-TM-2365 (2007).

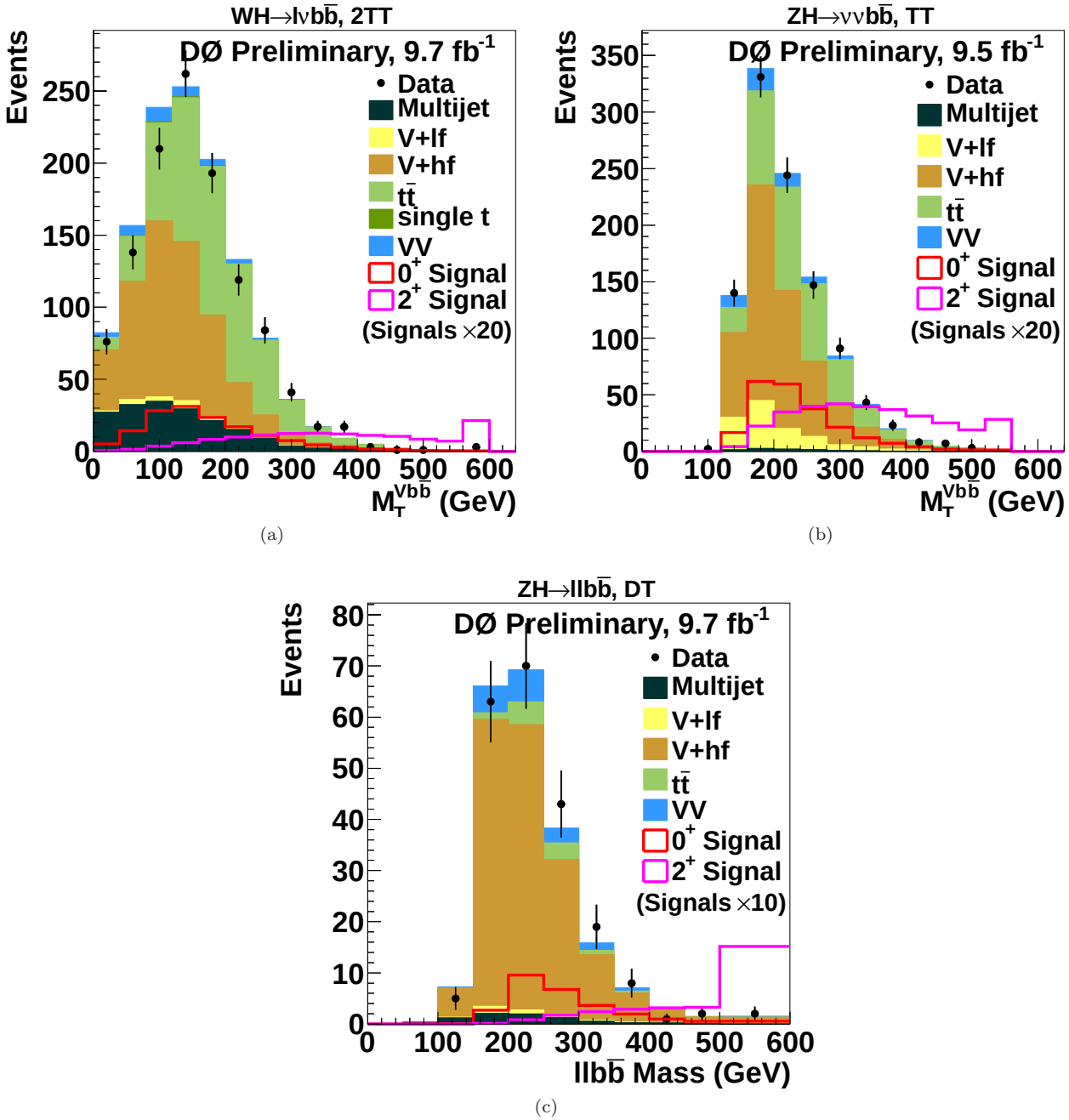

FIG. 2: Transverse mass of the: (a) $\ell\nu b\bar{b}$ system in the $WH \to \ell\nu b\bar{b}$ 2-tight-tag (2TT) channel, (b) $\nu\nu b\bar{b}$ system in the $ZH \to \nu\bar{\nu}b\bar{b}$ tight-tag (TT) channel, and (c) invariant mass of the $\ell\ell b\bar{b}$ system in the $ZH \to \ell\ell b\bar{b}$ double-tag (DT) channel. The $J^P = 2^+$ samples use the SM cross section. Overflow events are included in the last bin. All signals assume $M_H = 125$ GeV.

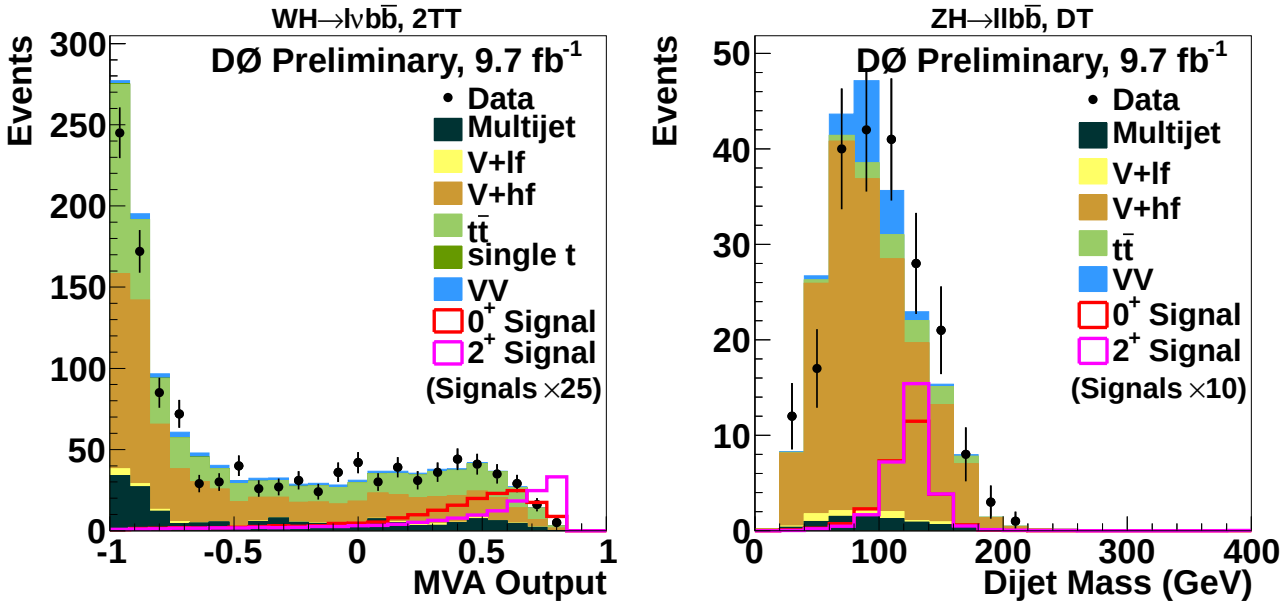

(a)

(b)

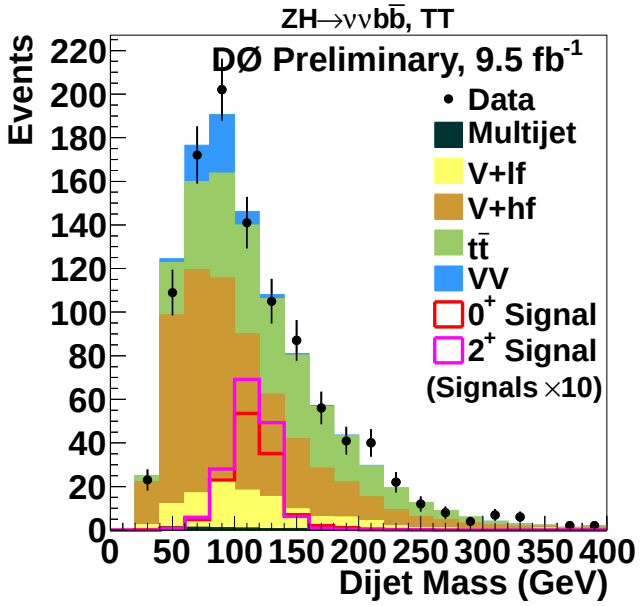

(c)

FIG. 3: (a) MVA output from the $WH \to \ell\nu b\bar{b}$ analysis in the 2-tight-tag (2TT) channel, and invariant mass of the two b-tagged jets from the (b) $ZH \to \ell\ell b\bar{b}$ analysis in double-tag (DT) channel and (c) $ZH \to \nu\bar{\nu}b\bar{b}$ analysis in tight-tag (TT) channel. The $J^P = 2^+$ samples use the SM cross section. All signals assume $M_H = 125$ GeV.

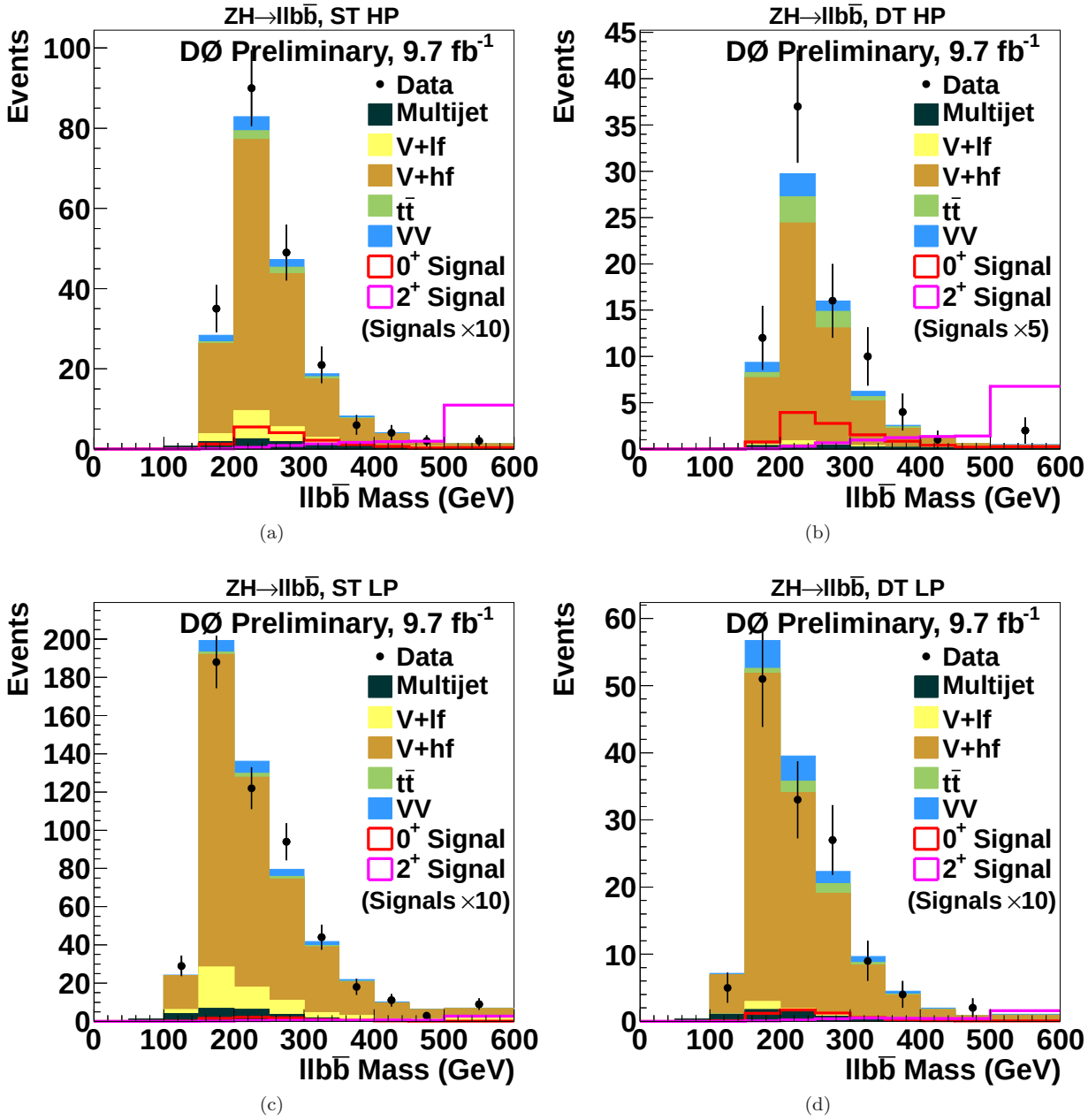

FIG. 4: Invariant mass of the $b\bar{b} + \ell\ell$ system in the $ZH \to \ell\ell b\bar{b}$ analysis in (a) single-tag high-purity (ST HP), (b) double-tag high-purity (DT HP), (c) single-tag low-purity (ST LP), and (d) double-tag low-purity (DT LP) channels. All signals are $M_H = 125$ GeV. The $J^P = 2^+$ samples use the SM cross section. Overflow events are included in the last bin. All signals assume $M_H = 125$ GeV.

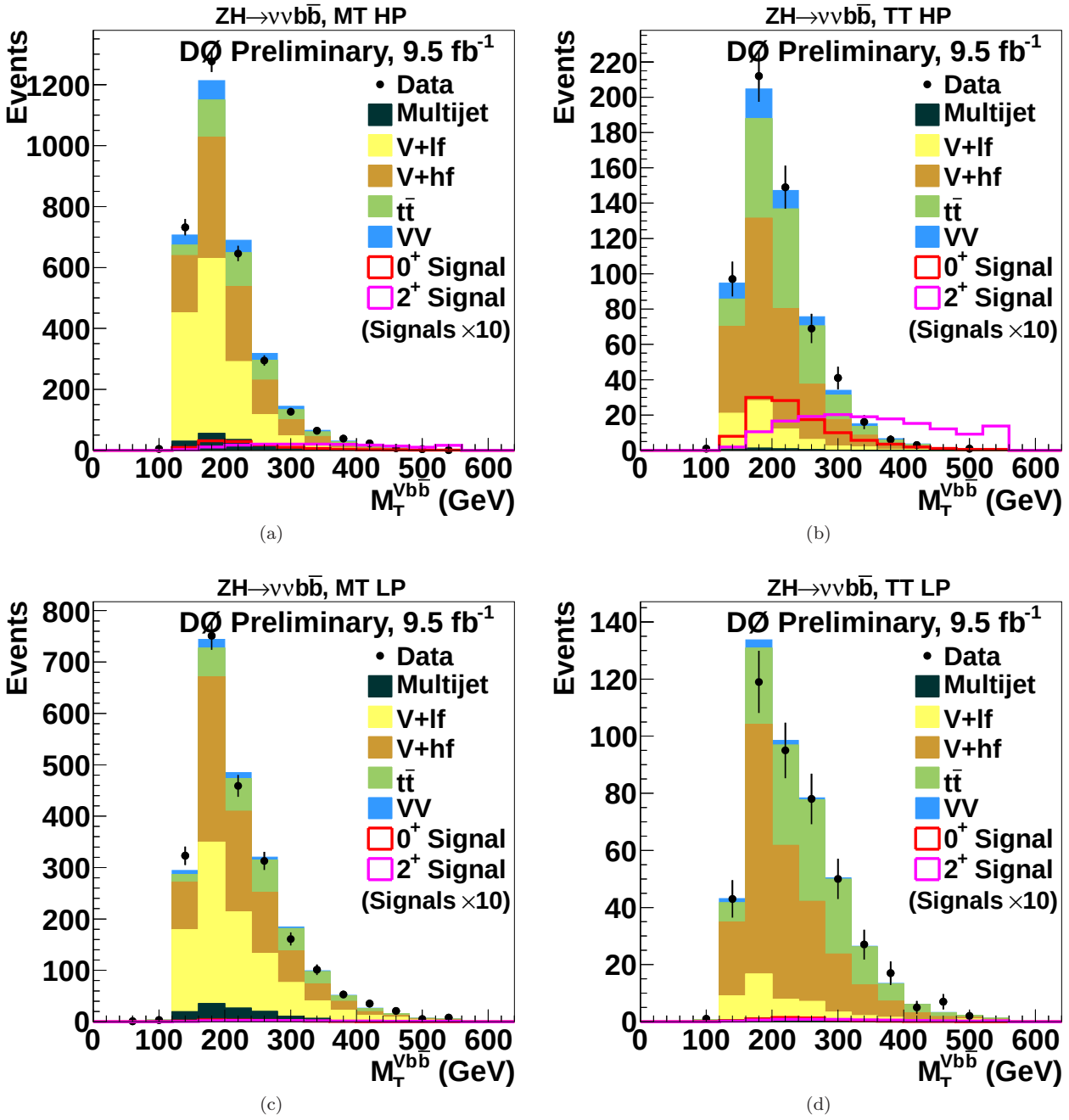

FIG. 5: Transverse mass of the $b\bar{b}+\not\!\!E_T$ system in the $ZH \to \nu\nu b\bar{b}$ analysis (a) medium-tag high-purity (MT HP), (b) tight-tag high-purity (TT HP), (c) medium-tag low-purity (MT LP), and (d) tight-tag low-purity (TT LP) channels. The $J^P = 2^+$ samples use the SM cross section. Overflow events are included in the last bin. All signals assume $M_H = 125$ GeV.

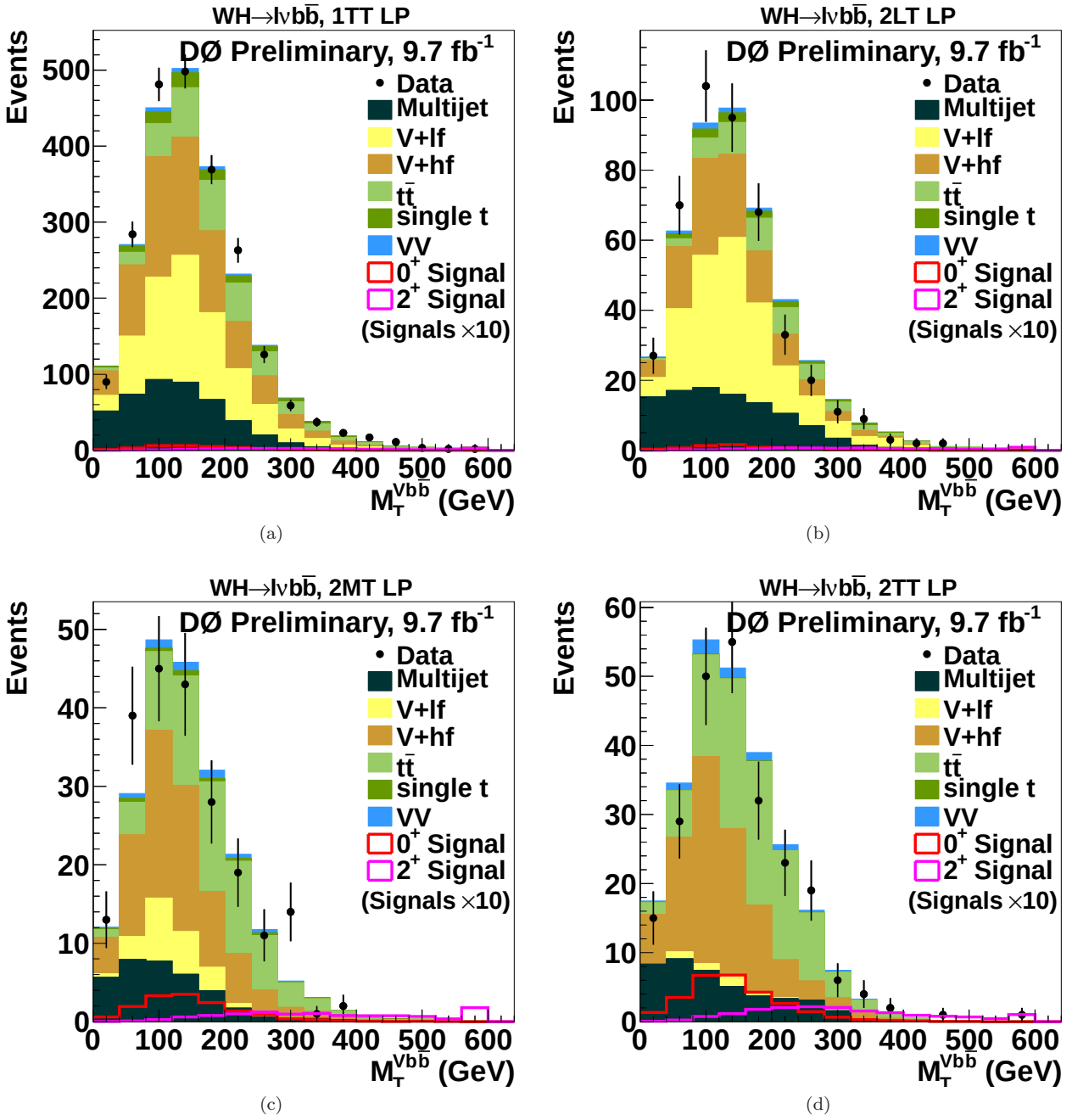

FIG. 6: Transverse mass of the $\ell + \not\!\!E_T + b\bar{b}$ system in $WH \to \ell\nu b\bar{b}$ analysis for events in the low purity (LP) region ($0 <$ MVA ≤ 0.5) for (a) 1-tight-tag (1TT), (b) 2-loose-tags (2LT), (c) 2-medium-tags (2MT), and (d) 2-tight-tags (2TT) channels. The $J^P = 2^+$ samples use the SM cross section. Overflow events are included in the last bin. All signals assume $M_H = 125$ GeV.

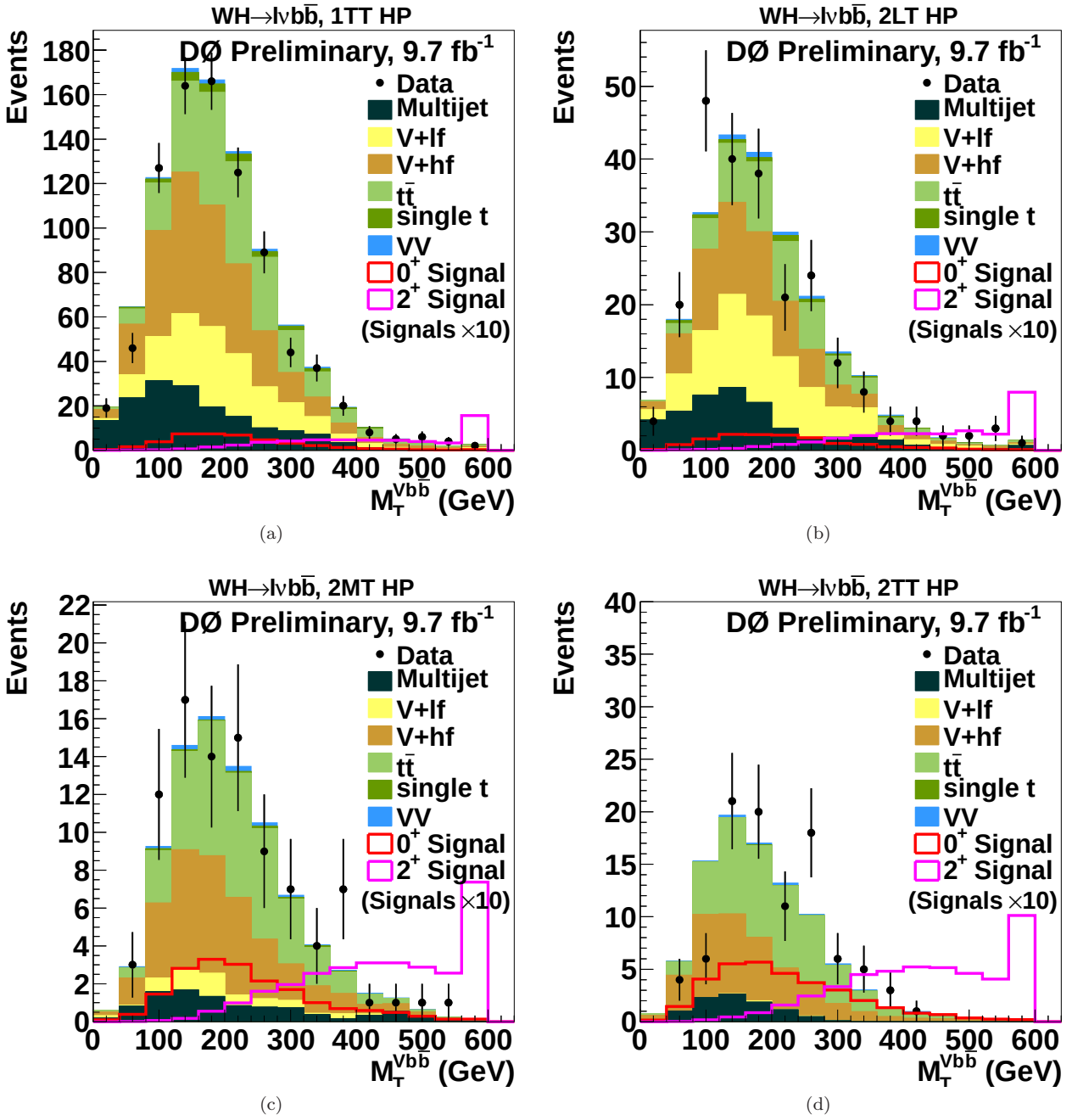

FIG. 7: Transverse mass of the $\ell + \not\!\!E_T + b\bar{b}$ system in $WH \to \ell\nu b\bar{b}$ analysis for events in the high-purity (HP) region ($0 <$ MVA > 0.5) for (a) 1 tight-tag (1TT), (b) 2 loose-tags (2LT), (c) 2 medium-tags (2MT), and (d) 2 tight-tags (2TT) channels. The $J^P = 2^+$ samples use the SM cross section. Overflow events are included in the last bin. All signals assume $M_H = 125$ GeV.

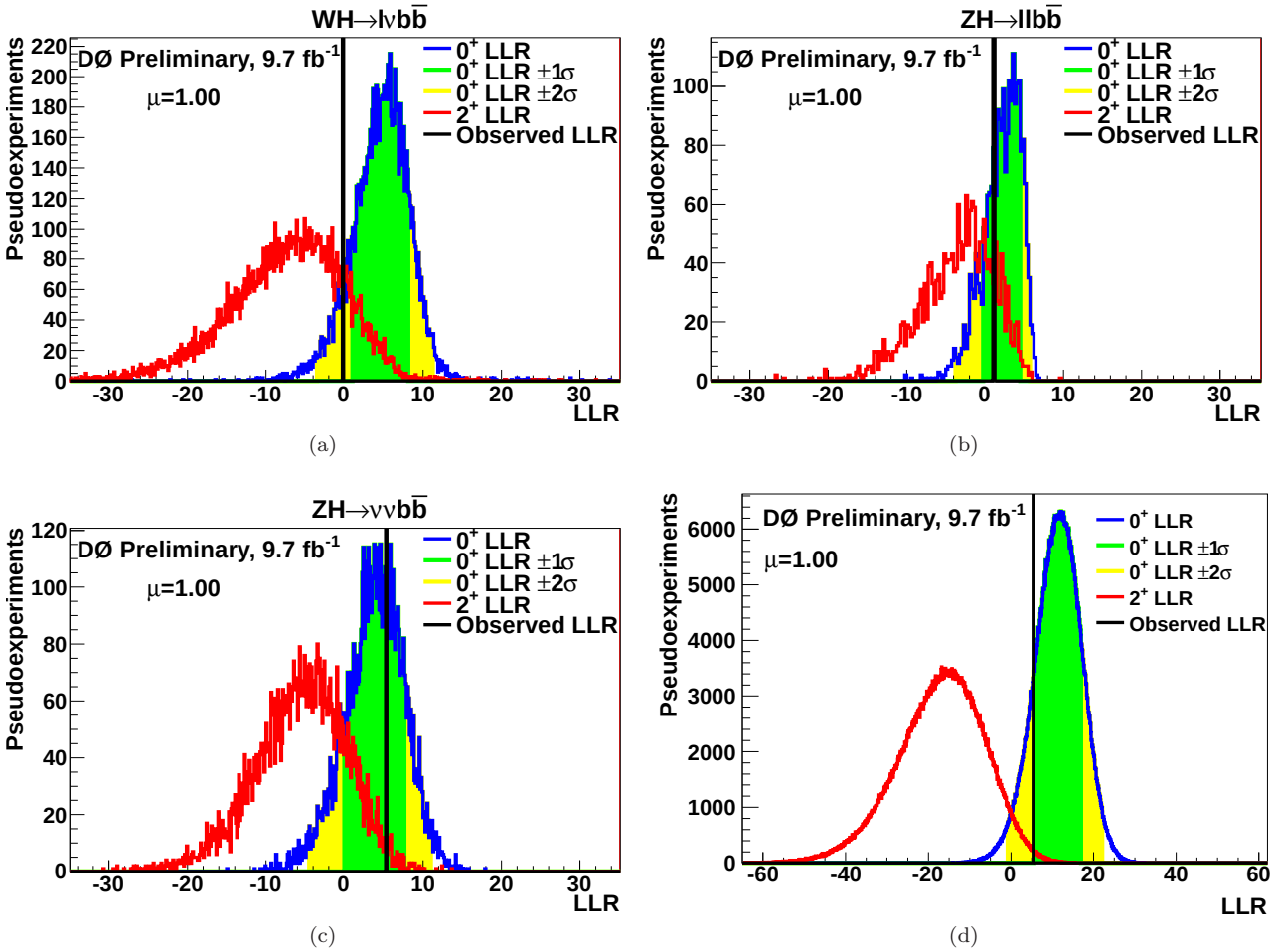

FIG. 8: LLR distributions when comparing the $J^P = 0^+$ and $J^P = 2^+$ hypotheses for the (a) $WH \to \ell\nu b\bar{b}$ analysis, (b) $ZH \to \ell\ell b\bar{b}$ analysis, (c) $ZH \to \nu\nu b\bar{b}$ analysis, and (d) combination. We normalize the $J^P = 2^+$ and $J^P = 0^+$ samples to the SM Higgs cross section at 125 GeV ($\mu = 1.0$). Black solid line represents observed value, while green and yellow area are 1 s.d. and 2 s.d. on the expectation from the null hypothesis H_0, which is in this case SM Higgs boson plus background.

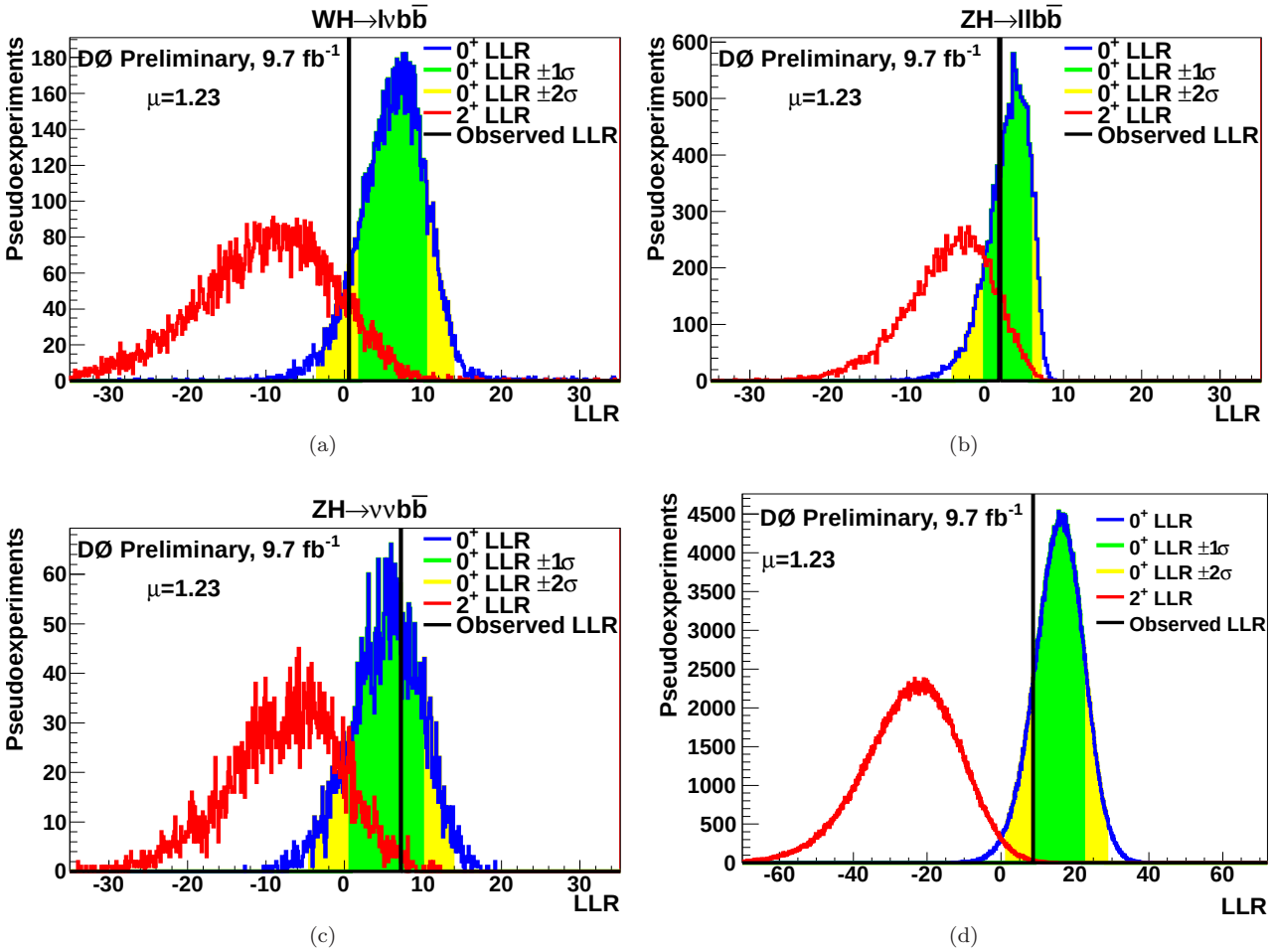

FIG. 9: LLR distributions when comparing the $J^P = 0^+$ and $J^P = 2^+$ hypotheses for the (a) $WH \to \ell\nu b\bar{b}$ analysis, (b) $ZH \to \ell\ell b\bar{b}$ analysis, (c) $ZH \to \nu\nu b\bar{b}$ analysis, and (d) combination. We normalize the $J^P = 2^+$ and $J^P = 0^+$ samples to the SM Higgs cross section at 125 GeV ($\mu = 1.23$). Black solid line represents observed value, while green and yellow area are 1 s.d. and 2 s.d. on the expectation from the null hypothesis H_0, which is in this case SM Higgs boson plus background.

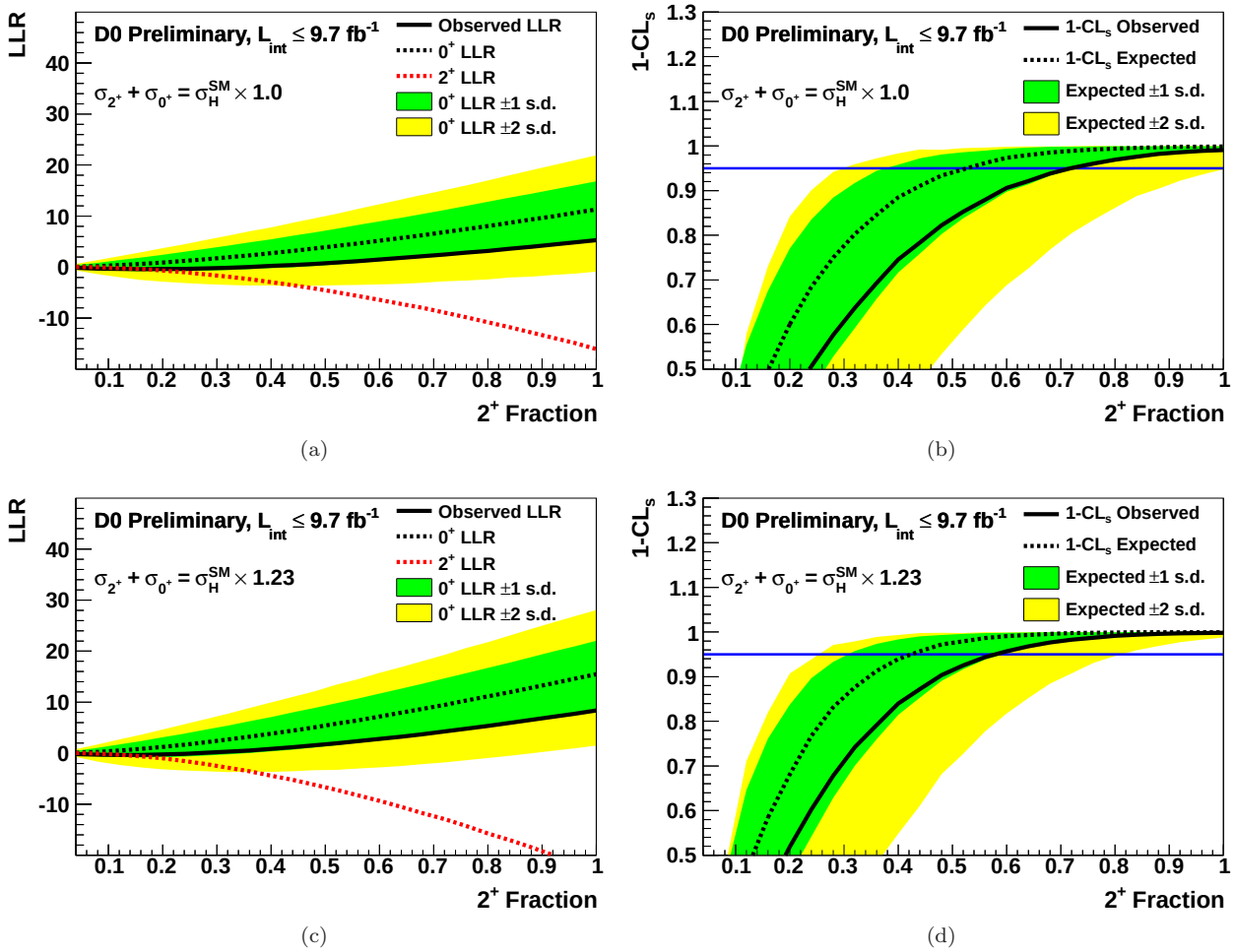

FIG. 10: Plot of (a) LLR for $\mu = 1.0$, (b) $1 - CL_s$ for $\mu = 1.0$, (c) LLR for $\mu = 1.23$, (d) $1 - CL_s$ for $\mu = 1.23$, as a function of the $J^P = 2^+$ signal fraction f_{2^+} for all channels combined. We define H_1 to be the sum of background, the $J^P = 2^+$ signal normalized to $\mu \times \sigma_{SM} \times f_{2^+}$, and the $J^P = 0^+$ signal normalized to $\mu \times \sigma_{SM} \times (1 - f_{2^+})$. We define H_0 to be the sum of background and the $J^P = 0^+$ signal normalized to $\mu \times \sigma_{SM}$ (i.e. a pure $J^P = 0^+$ signal.)